Thin-Walled Structures 144 (2019) 106277

Contents lists available at ScienceDirect

Thin-Walled Structures

journal homepage: www.elsevier.com/locate/tws

Full length article

A numerical study on the influence of internal corrugated reinforcements on the biaxial bending collapse of thin-walled beams

Rade Vignjevic[a], Ce Liang[a], Kevin Hughes[a,*], Jason C. Brown[b], Tom De Vuyst[c], Nenad Djordjevic[a], James Campbell[a]

[a] Dynamic Response Group, Department of Mechanical and Aerospace Engineering, Brunel University London, Granta Park, Great Abington, Cambridge, CB21 6AL, UK
[b] Applied Mechanics, C/o School of Aerospace, Transport and Manufacturing, Cranfield University, Beds, MK43 0AL, UK
[c] School of Engineering and Computer Science, University of Hertfordshire, Hatfield, AL10 9AB, UK

ARTICLE INFO

Keywords:
Uniaxial and biaxial bending collapse
Post buckling and deep collapse
Corrugated tube reinforcement
Passive energy absorption concept
Simulation led design

ABSTRACT

The Heat Treatment Forming and in-die Quench (HFQ) process allows for manufacturing of more complex geometries from Aluminium sheets than ever before, which can be exploited in lightweight automotive and aerospace structures. One possible application is manufacturing thin walled beams with corrugated internal reinforcements for complex geometries.

This work considers different internal reinforcements (C-section and corrugated) to improve the energy absorption properties of thin walled rectangular beams under uniaxial and biaxial deep bending collapse, for loading angles ranging from 0 to 90 deg, in 15° increments. Using LS-DYNA simulations experimentally validated through unreinforced metallic tubes under quasi-static bending collapse, the finite element results demonstrate the stabilising effect of the reinforcements and an increase in the buckling strength of the cross section.

Corrugated reinforcements showed a greater potential for increasing specific energy absorption (SEA), which was supported by investigating key geometric parameters, including corrugation angle, depth and number. This favourable response is due to an increased amount of material undergoing plastic deformation, which consequently improves performance of the beam undergoing post buckling and deep collapse. This concept is applicable to vehicle and aircraft passive safety, with the requirement that the considered geometries are manufacturable from Aluminium Alloys sheet only, using the HFQ process.

1. Introduction

Vehicle passive safety is achieved mainly through careful design of the vehicle body structure, as structural collapse during a crash is caused by loads substantially different in direction, intensity and place of application from normal service loads. Deformation begins with an initial elastic deformation that increases linearly until plastic deformation, buckling, tearing and joint failures develop. In this process, the stiffness of the structure decreases with each local failure, whereby each local overloading causes a redistribution of internal loads (due to the highly redundant nature of a vehicle body), to components whose load carrying capacity is still not fully exhausted.

Many elements of a vehicle body primary structure are thin walled beams, which buckle elastically before full plasticity of the section takes place in a crash event. These beams, intended to work primarily in bending, have local failure modes very similar to mechanism hinges, in the sense that relative rotation of two elastically deformed segments of a collapsed beam takes place about a localised area of plastically deformed, buckled or fractured material. The energy absorption/load carrying capacity of these beams are typically characterised by moment vs. rotation curves, which are of great importance in vehicle safety design. A good energy absorber of this type should have sufficient strength and maintain its resistance through fairly large angles of hinge rotation, whereby the angles considered depend upon the collapse mechanism and allowable survival space.

The elastic properties of a beam depend upon design, manufacturing process and material. With pressed sheet welded beams, the effective bending stiffness may also vary significantly depending on the characteristics of the manufacturing process (spot weld pitch, quality of bonding, material anisotropy, etc.) and it is generally below the value predicted by beam theory. The deflections of open section beams also depend on the position of load with respect to the shear axis and on warping inhibition at its ends. The effect of shear may become important in very short (deep) beams and in some aircraft elements with

* Corresponding author.
E-mail address: kevin.hughes@brunel.ac.uk (K. Hughes).

https://doi.org/10.1016/j.tws.2019.106277
Received 21 February 2019; Received in revised form 7 June 2019; Accepted 26 June 2019

stiffeners, shear lag effect may also have to be included. For this paper, the rectangular beams considered can be treated adequately using beam theory.

The maximum bending strength of a rectangular section beam is usually achieved at the point where the beam starts collapsing, which may be initiated by:

1. Plastic yielding of the material over the whole section;
2. Plastic yielding of the material over part of the section, combined with elastic or inelastic buckling of some other segments of the section;
3. Plastic yielding of the material over part of the section, combined with material separation over another segment of the same section.

The first case is common in stable section beams made of a ductile material. The second collapse form applies to beams that buckle locally before the maximum moment is achieved. Local buckling may be elastic or inelastic, depending on the stability of the compressed segments of the section. Most of the beams used in vehicle bodies represent thin walled beams, so buckling has an important effect on their collapse behaviour. The third possibility is not typical in ductile materials, except in special cases of stress or strain concentration.

The collapse mechanism of rectangular or square section beams was analysed in detail by Kecman, who showed that the maximum bending strength of a rectangular thin walled beam is equal to, or less than the fully plastic moment, depending upon the stability of the section walls [1]. Kecman observed that when the compression cross section flange buckles, the loads are redistributed to its edges, reducing the 'effective width" of the flange. Collapse start coincides with maximum strength, which occurs when the effective width of the section goes plastic. Fully plastic moments may only be safely assumed if the critical elastic stress of the flange is approximately three times greater than the yield stress of the material.

This paper proposes an approach for improvement of strength and energy absorption of rectangular cross section beams based on corrugated inserts. These inserts stabilise and increase buckling strength of the cross section. In addition, the inserts increase the amount of material undergoing plastic deformation and consequently improve beam performance during post buckling and deep collapse.

This paper is presented in seven sections with section two reviewing bending collapse of closed, thin-walled beams with reinforcements, in which only a modest body of knowledge could be found. As this paper focuses on biaxial bending of rectangular beams, this is discussed in detail in section three, where the experimental data was used to validate the numerical models developed. Section four considers the influence of reinforcement geometry on uniaxial and biaxial bending collapse through simulation of two different loading boundary conditions, namely fixed displacement plane and fixed moment plane to investigate how the choice of boundary conditions can apply constraints on the beam and influence collapse. A parametric study of corrugated reinforcements presented in section five, considered a range of corrugation geometries, including corrugation depth, flange angles and number of corrugations. The paper concludes with the key findings for the concept of corrugated internal reinforcements to improve the energy absorption properties of thin walled rectangular beams under uniaxial and biaxial deep bending collapse.

2. Review of bending collapse of closed thin-walled beams with reinforcements

From the literature, several approaches to increase energy absorption of thin-walled structures subjected to bending loads have been investigated, namely through:

(i) Filling thin-walled beams with cellular materials such as foams and honeycombs [2–9].
(ii) Adopting multi-cell cross-sectional profiles [10–12].
(iii) Introducing small features to sheet metal to reinforce local regions [13–15].
(iv) Combination of methods above [16–18,26].

The concept of filling beams under bending loads with foams was proposed by Santosa and Wierzbicki, who claimed ultralight metal fillers could achieve a higher energy absorption to weight ratio than thickening the walls [2]. Zarei and Kroger used experimental and numerical methods to optimise the specific energy absorption of foam-filled square section beams [3]. Optimisation of sectional profiles was extended by Zhang, who used analytical and numerical approaches to investigate the bending behaviour of closed foam-filled, twelve right-angle section beams around two perpendicular axes [4]. It was claimed that using the proposed analytical approach, the cross section dimensions, thickness and material can be quickly selected in the early design phase [4].

Xiao et al. presented a parametric study to optimise the energy absorption of functionally graded foam-filled bumper beams and used multi-objective optimisation algorithms to consider parameters including density gradient, density range and wall thickness [5].

Durate et al. focused on the manufacture and bending behaviour of in situ foam-filled beams, who reported that comparing to ex situ foam-filled beams, in situ foam-filled beams had a more stable and predictable behaviour under bending loads, although the energy absorption capacity was lower due to the manufacturing process [6]. Zhang et al. proposed to use small aluminium alloy boxes as beam fillers to reinforce local regions of beams [7]. The proposed configurations were reported to be more cost-effective, easily available and more effective in improving the bending resistance of thin walled beams, when compared to foam-filled beams [7].

In addition to foam, honeycomb fillers also showed great potential. Liu et al. presented a preliminary investigation into the behaviour of square beams with aluminium honeycomb fillers under dynamic bending loads [8]. Xiao et al. extended this study by investigating the influence of loading velocity, wall thickness, fibre direction and stacking sequence of carbon fibre reinforce plastic (CFRP) beams [9]. In both studies, aluminium honeycomb fillers improved the specific energy absorption, as well as stabilised the failure mode [8,9].

In contrast to filling beams, an alternative approach is to partition and add internal (reinforcing) webs to make the cross section 'multi-cell'. Wang et al. performed experiments and numerical simulations to investigate the influence of various parameters on the response of multi-cell square section beams to bending loads [10], and developed theoretical predictions for design [11]. Zhang et al. proposed the concept of embedded multi-cell beams, which offered increased flexibility and cost-effectiveness in manufacturing over previous multi-cell beams, as they do not necessarily require new moulds when the sectional profiles change [12]. Despite multi-cell beams having significantly higher specific energy absorption than their empty counter parts, it should be noted these beams are usually manufactured by extrusion moulding, which brings its own limitations/challenges.

Introducing small features for local reinforcement can increase bending resistance, as Teter and Kolakowski reinforced the central web by introducing one corrugation and investigated the buckling mechanism under bending and torsion loads [13]. Obst et al. reinforced the side flanges by introducing an extra layer of corrugated sheets [14]. However, both studies only focused on open-section beams and did not include the post-buckling stage where the majority of energy absorption takes place. Liang et al. studied the response of square beams with dimpled surface to lateral impact loads, and suggested the use of small dimples can effectively increase crush efficiency under lateral impact [15].

The above design approaches were not only studied independently, but also combined. Magnucki and Paczos compared the performance of channel beams with corrugated side flanges and fillers [16]. Magnucka-

Blandzi et al. extended this work by investigating more corrugation profiles and locations [17]. As with Teter [13] and Obst [14], these studies also did not include the post-buckling stage. Yin et al. combined the concepts of multi-cell sections and foam materials and investigated the bending behaviour under lateral impact loads, using the complex proportional assessment (COPRAS) multi-objective analysis method [18]. The authors concluded that a 3 × 3 multi-cell foam-filled beam provided the optimum configuration under lateral impact loads. In a separate study, Guo investigated the dynamic three point bending response of foam filled single and double tubes and experimentally demonstrated that double filled foam tubes offered the greatest specific energy absoprtion capacity over traditional foam filled single tubes [26].

To date, reinforcing beams by extensively using corrugated structures has not been previously presented in the literature. Moreover, adopting corrugated reinforcements to improve bending crashworthiness of beams also has not been considered. This paper addresses this gap, by developing a proof of concept to improve the specific energy absorbed when compared to unreinforced, square tubes under biaxial bending.

3. Biaxial bending collapse of unreinforced square sectional beams

This section reviews the test configuration used by Brown to investigate the quasi-static, biaxial bending collapse of square-cross-sectional beams, under two different types of loading conditions [19,20]. The tests applied deflection increments, or bending moments in the 0, 15, 30 and 45° directions relative to the principal axes of the cross section. The forces recorded during the formation of a plastic hinge were used to validate the baseline FEA model developed.

3.1. Test setup

Square cross section beams were manufactured from commercially available cold-drawn seam welded steel, with outer dimensions of 38 × 38 mm and a wall thickness of 1.2 mm. For all tests, the beams were oriented to ensure the seam weld was always under tension. Engineering stress-strain curves were determined from tensile coupons taken in the direction of rolling and tested according to BS 18, resulting in the nominal properties in Table 1.

The choice of boundary conditions can apply constraints on the beam and influence collapse. Brown therefore investigated two different constraint conditions [19], namely:

1. The axis of collapse hinge rotation being in a fixed direction, allowing the moment components to cause collapse to be measured (i.e. fixed displacement plane boundary condition)
2. The axis of the resultant hinge moment was in a fixed direction, allowing free deflections and forces to be measured (i.e. fixed moment plane boundary condition)

These two configurations are shown in Fig. 1 and Fig. 2, and developed based on the findings of Kecman [1] and Miles [21], who recommended loading the beams as cantilevers, as this offered a simpler, more reliable arrangement over four point bending, particularly for large hinge rotations. Therefore, each beam was cast in concrete as a result.

Table 1
Geometry and mechanical properties for the square cross-sectional beams.

	Dimensions	Units
Outer cross-section	38 × 38	mm
Wall thickness	1.2	mm
Young's Modulus	190	GPa
Yield strength	292	MPa
Ultimate strength	337	MPa
Elongation	20	%
Beam length	720	mm

The first boundary condition forced the cantilever to deflect in a given fixed plane (Fig. 1). According to Brown, this was achieved by mounting pre-tensioned sidestays between the top end of the beam and spherical anchor pivots (Points D and G), which were equally distanced from the fully fixed end of beams. Deflections were applied by a horizontal, rigidly mounted screw-jack (Point C) connected to the top end of the beam via a ball joint [19].

The second boundary condition applied the end load in a constant direction that remained horizontal throughout the test (Fig. 2). Based on Brown's description, a load link was attached to the free end of the beam via a ball joint, which included a load cell, whilst the other end of the link was mounted onto a roller that was able to move laterally. Allowing lateral movement eliminated any additional constraints applied to the beam, due to self-alignment of the load link in the required directions [19].

Another key requirement for the second boundary condition was to maintain a horizontal load, achieved by mounting the roller track to a H-frame, which was free to rotate at its base through pin joints (connecting the track to Point G in Fig. 2). The height of the H-frame was set to the height of each beam tested, which in turn, was connected to a screw jack that applied the displacement increments. Tip deflection was measured using two linear displacement potentiometers, aligned laterally and longitudinally.

To determine the biaxial bending response, displacement increments (or moments) were applied at 15° increments from 0 to 45°, relative to the longitudinal axis of the beam, with two tests per orientation. For both boundary conditions, clamps and an insert were fitted at the top end of tubes to locally reinforce and prevent any warpage of the cross-section under load, to which the displacement controlled loading was applied. For analytical purposes, the top of the tube was considered effectively rigid. Photographs of the collapsed tubes are presented in Fig. 3.

4. Baseline FE model development

This section reviews the development of an appropriate model for concept development using LS-DYNA (R10) MPP single precision solver [22]. In order to simulate a quasi-static displacement controlled test using explicit time integration (as computational cost is proportional to the number of elements and roughly inversely proportional to the smallest characteristic length in the FE model), a commonly used technique is to “accelerate” the loading process to allow the simulation to be performed in the shortest time period and avoiding inertial effects affecting structural response [23]. This approach was adopted in this research resulting in a constant loading rate of 0.5 m/s, which ensured inertial effects were low (i.e. Kinetic Energy < 1% of the Internal energy).

Key features of the analysis include:

- Tube geometry was idealised and the rounded corners in the actual cross-section (due to the folding process) were disregarded. Fully integrated shell elements (midplane) with a uniform element size of 2 mm (for mesh convergence) and a bilinear elastic-plastic material model using properties in Table 1 were assigned.
- An automatic single surface contact algorithm (segment based) with contact thickness equal to half the wall thickness. Coefficients of static and dynamic friction were 0.74 and 0.57 respectively [24].
- Base nodes were fully constrained to represent the concrete casting used in the experiments.
- Cross-sectional forces were calculated from the base row of elements.
- In order to prevent local deformation of the cross-section under

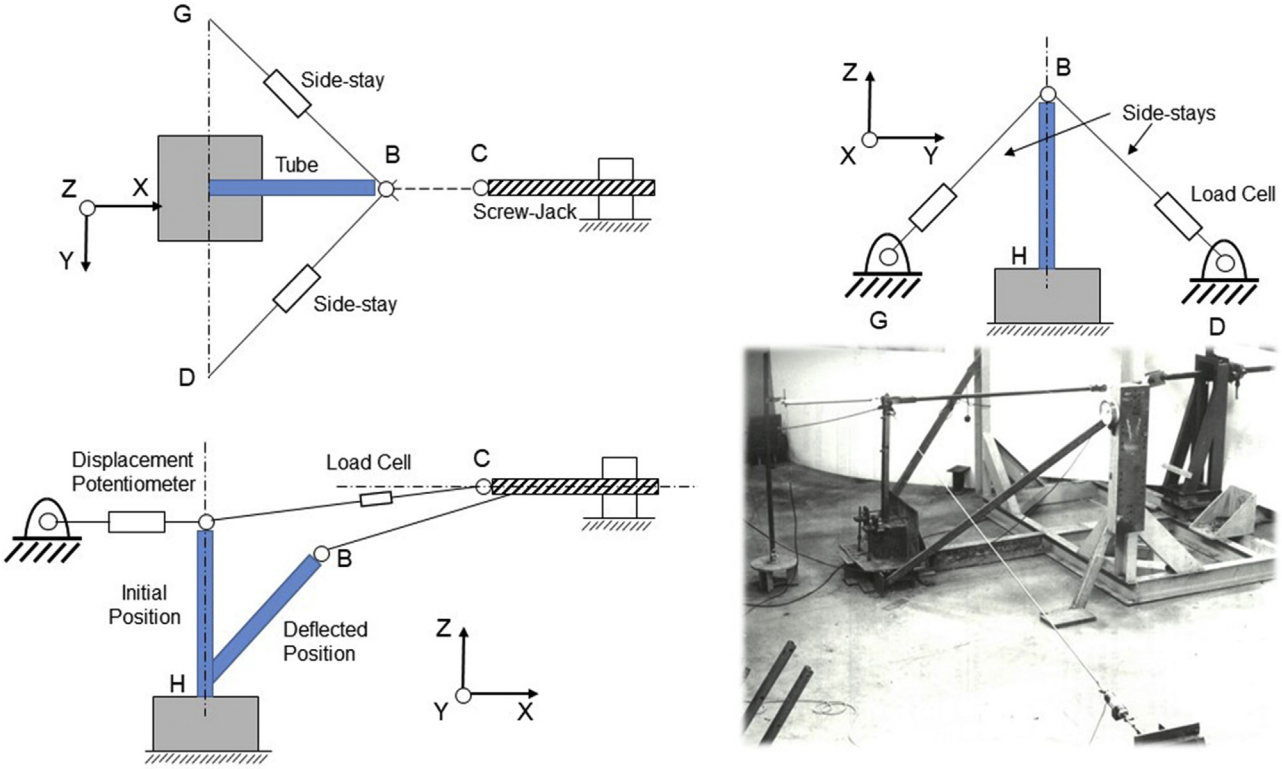

Fig. 1. Boundary Condition 1 (fixed displacement plane) that ensured the axis of collapse hinge rotation was in a fixed direction; Photograph is of the actual test setup [19].

load, the top 10 mm of the beam was defined as a rigid material, to which displacements were extracted.

- Using a local (velocity) vector to define the four different loading directions, for boundary condition 1, out of plane motion in the loading direction was constrained, whereas for boundary condition 2, no constraints were applied.

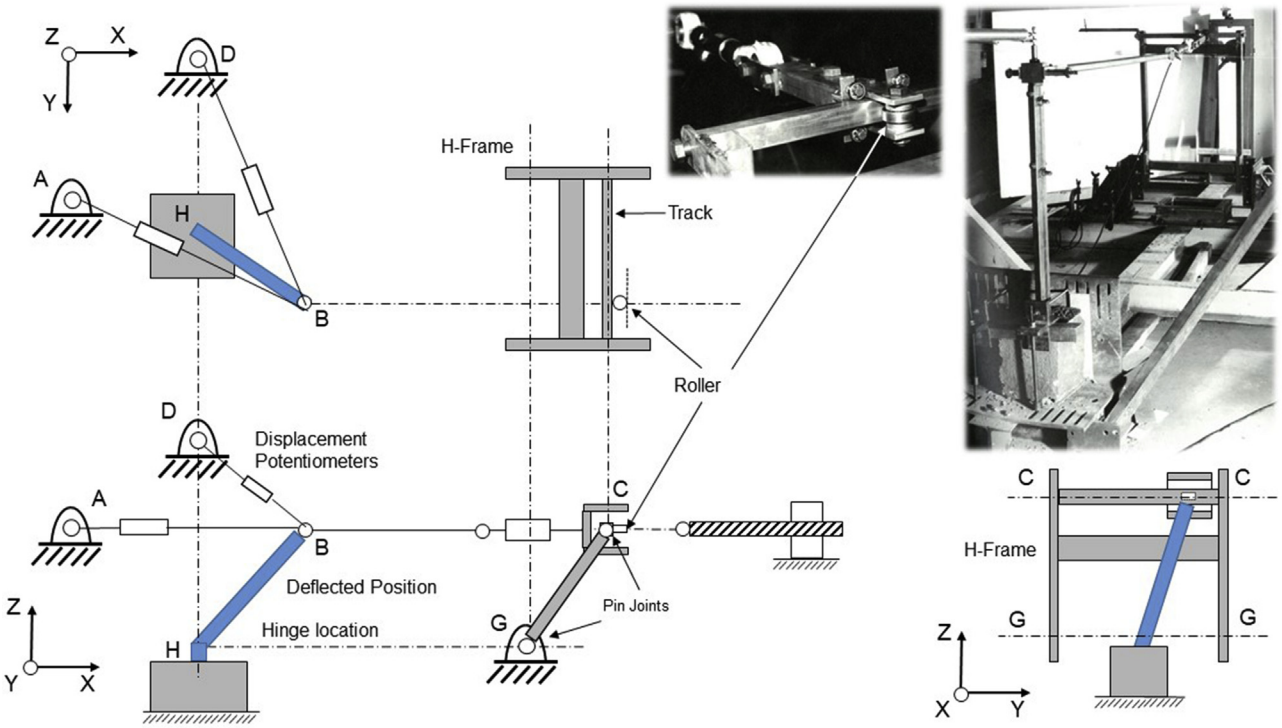

Fig. 2. Boundary Condition 2 (fixed moment plane) ensuring the axis of resultant hinge moment was in a fixed direction; Photographs are of the actual test setup [19]. (a) – Boundary Condition 1 (Fixed displacement plane). (b) – Boundary Condition 2 (Fixed Moment Plane).

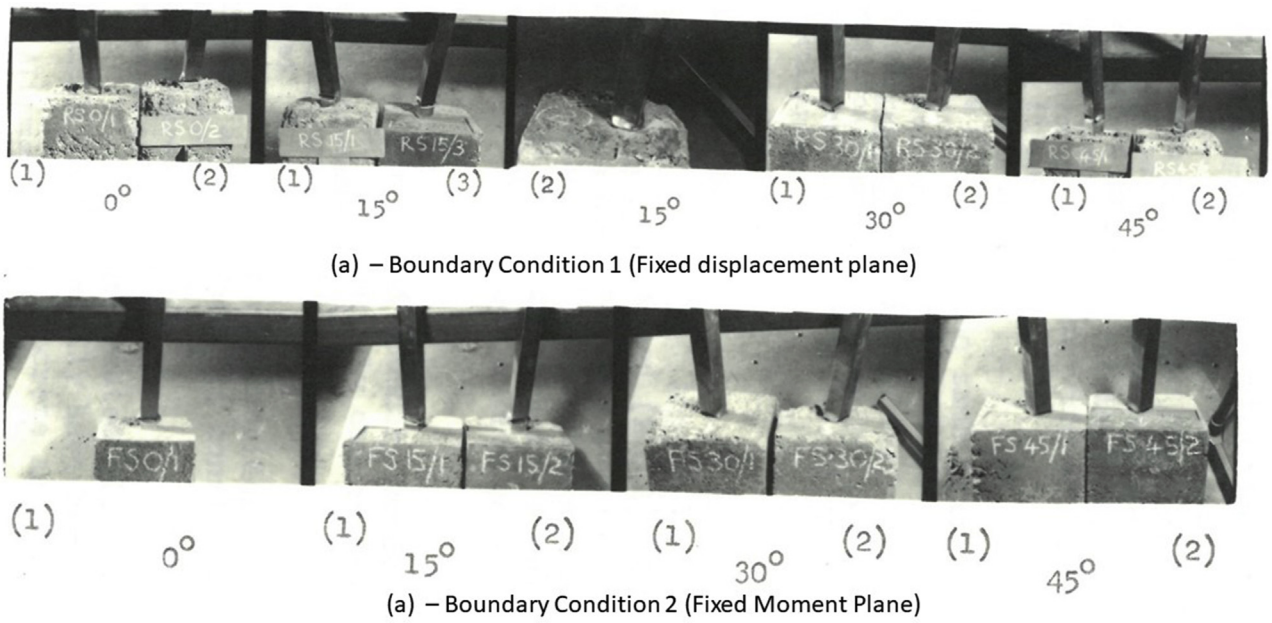

Fig. 3. Collapsed Square Section tubes for loading angles 0, 15, 30 and 45° [19].

4.1. Validation of baseline FE model

A sequence for plastic hinge formation in the 0° loading direction is presented in Fig. 4. To support validation, the plastic collapse moment, M_p, was calculated for this uniaxial loading case using Eq. (1), where σ_Y represents yield strength, assuming a symmetric distribution of tensile and compressive regions [25]. Using the properties in Table 1, the converged FEA prediction overestimates the theoretical calculation by +6% (M_p = 712Nm, $M_{p,FE}$ = 755Nm), providing confidence with the modelling approach and an acceptable computational cost (~35 min on 24x Intel Xeon 2.5 GHz CPUs).

$$M_P = \frac{1}{4}\sigma_Y [W^3 - (W - 2t)^3] \tag{1}$$

where W is the width of the cross-section and t is the wall thickness.

For both boundary conditions, the resultant force-displacement curves for test and simulation across all four loading directions are shown in Fig. 5 and Fig. 6. Only data corresponding to a consistent response are included in this paper (i.e. an inward plastic hinge formed on the compression face of the tube), whereas the complete data set is available in Brown [19]. Initial problems reported by Brown included alignment difficulties for both boundary conditions. In Boundary Condition 1 for example, ensuring a repeatable, fixed displacement plane through pre-tensioned side stays was essential, as any sag occurring during beam collapse was attributed to causing scatter in results, whereas for Boundary Condition 2, careful alignment of the roller track, loading angle and position of displacement potentiometer anchor points required careful attention.

In general, good agreement was found in terms of elastic stiffness, magnitude and duration of peak collapse moment and subsequent decay between test and simulation across both boundary conditions. A discrepancy (and scatter between test) was observed for the 45° loading angle for Boundary Condition 1, as the cross-section receives considerable reinforcement from the corner. Here, the loading angle coincides with the symmetrical diagonal axis of the section, which can have an erratic effect on the normality condition[1] [20]. In addition, the FE model overestimates peak moment (Fig. 6) for Boundary Condition 2. Both issues are attributed to differences in tube corner idealisation, as the FE model does not incorporate rounded corners (in order to reduce computational run time). Assuming the corners to be a perfect right angle was an appropriate geometric simplification, as the focus of the model was to capture the post buckling collapse.

Comparing the energy absorbed between test and simulation (Table 2), the level of predictive accuracy is within 2% across all loading angles for boundary condition 2 (fixed moment plane). For boundary condition 1 (fixed displacement plane), predictive accuracy was ~8% of the average value. From test, the scatter in test data for boundary condition 2 is small, due to the self-alignment of the loading direction (repeatable), whereas for boundary condition 1, maintaining a fixed displacement plane under bending collapse is more challenging and reflects the larger scatter observed, as reported by Brown [20]. Therefore, the FE modelling approach was capable of predicting the response of thin-walled beams under biaxial bending and can be reliably used to investigate the influence of internal corrugated reinforcements against these baseline (unreinforced) results.

5. Alternative designs: influence of reinforcement

The influence of internal reinforcement in terms of specific energy absorption will be demonstrated using two reinforcement designs (Fig. 7) and compared against an unreinforced tube. For all simulations, a standard tube length of 720 mm, in which an internal 300 mm reinforcement (aligned with the tube base) was inserted. Quasi-static bending loads were applied from 0 to 90° in 15° increments with a coordinate system that ensures the widest surface of the reinforcement is always subject to compression, for both loading boundary conditions. The inserts and the definitions for the loading directions are illustrated in Fig. 7. The reinforcement length was sufficiently sized to avoid any boundary effects, by ensuring the plastic hinge forms in the reinforced region of the tube.

It was assumed the tube and reinforcement were connected by three longitudinal welding lines located at the midpoint of each reinforced face (circled regions in Fig. 7). This connection was achieved in the numerical model using shell elements, providing a direct connection (no failure) between the elements representing the tube and reinforcement (Fig. 8). Both reinforcements used a uniform wall thickness

[1] (Normality Condition states the deflection direction is equal to the direction of the normal of the yield locus at the point where the plastic moment makes contact; a general principle for sections that fail by bulk plastic deformation).

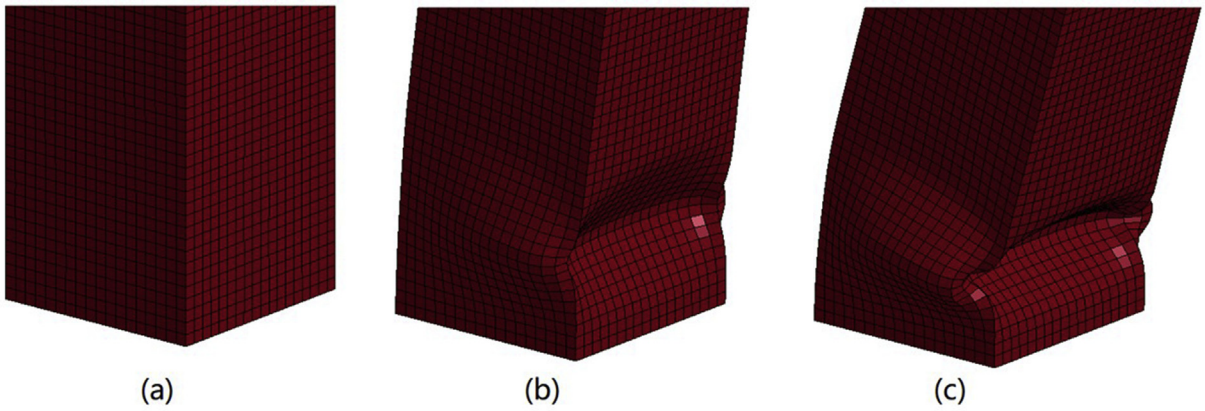

Fig. 4. Hinge formation at rotations of (a) 0, (b) 0.15 and (c) 0.2 rad for 0° loading direction.

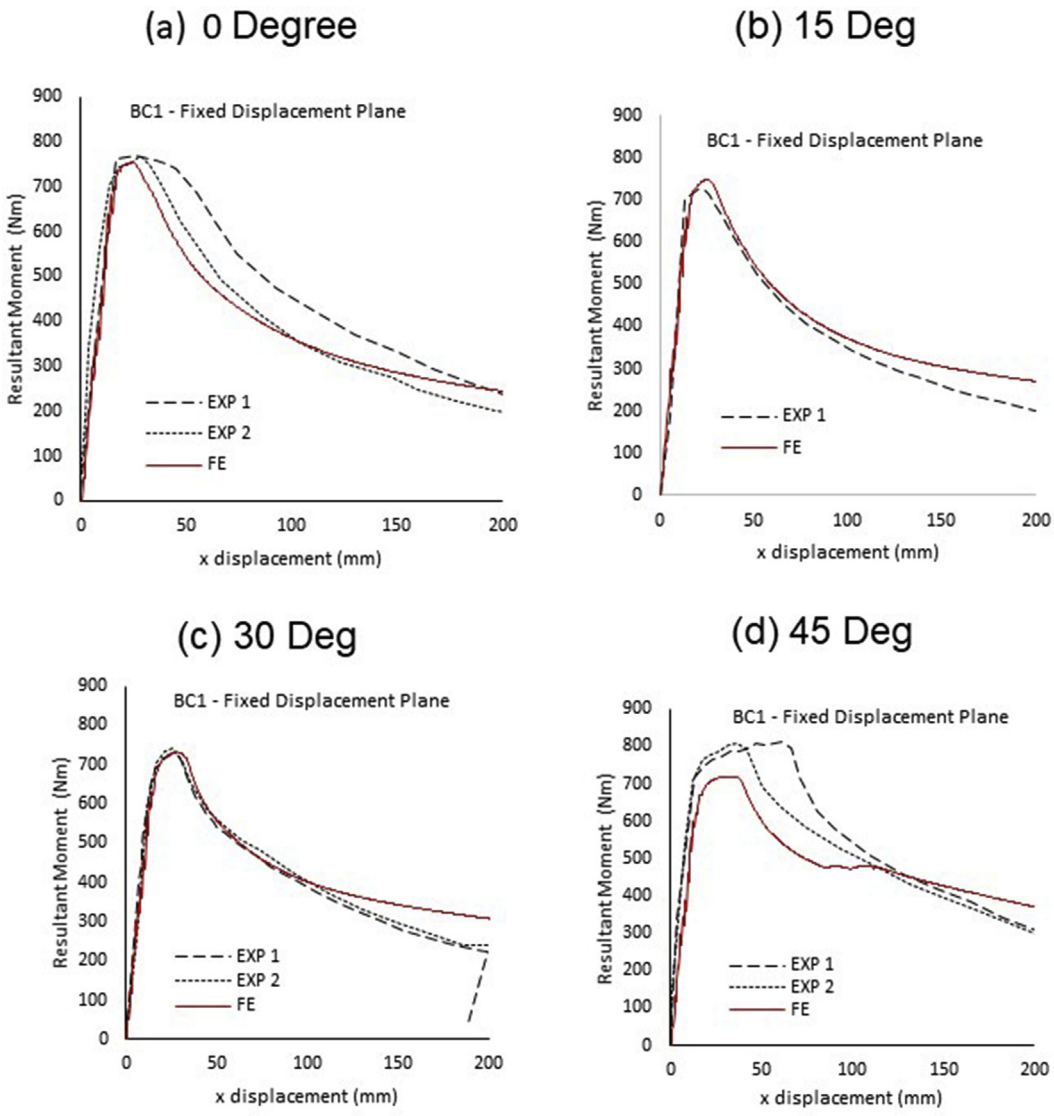

Fig. 5. Moment – displacement curves for boundary condition 1 (i.e. fixed displacement plane).

of 1.2 mm with full dimensions defined in Table 3. For the baseline configuration, the length of each edge of a single corrugation was 4 mm for a corrugation angle of 45°.

The longitudinal connections between insert reinforcement and outer tube were located along the centre line of the three external outer tube faces, whereby the coincident nodes were equivalenced (i.e. no failure allowed).

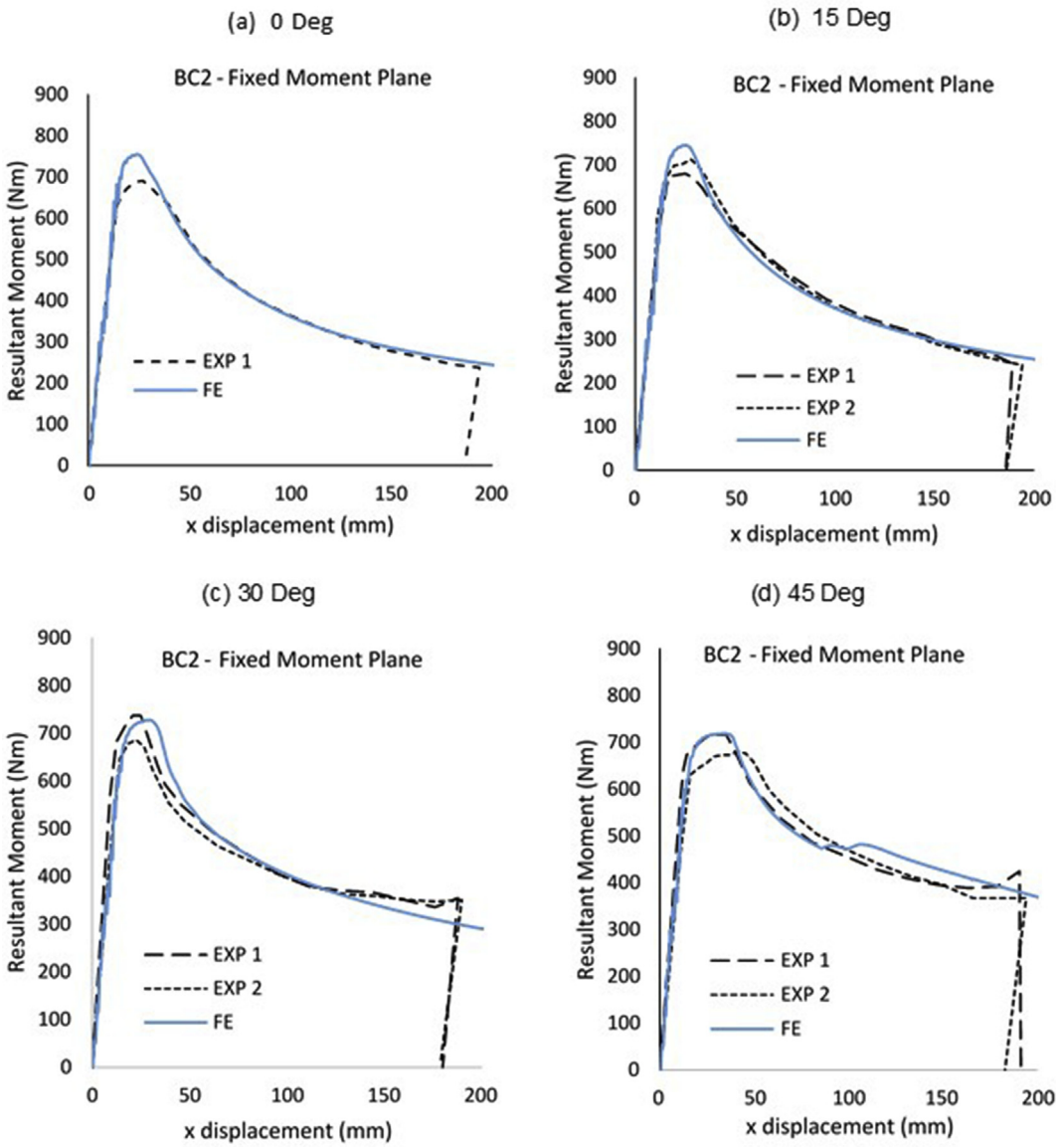

Fig. 6. Moment – displacement curves for boundary condition 2 (i.e. fixed moment plane).

Table 2
Experimental and numerical energy absorption (at rotation = 0.2 rad).

Boundary condition	Loading direction	EXP 1 (J)	EXP 2 (J)	EXP ave. (J)	FE (J)	%Error wrt Average
Fixed displacement plane	0°	111.3	99.0	105.1	92.9	−11.6%
	15°	89.9	N/A	89.9	94.3	+4.8%
	30°	95.8	97.7	96.7	98.2	+1.5%
	45°	128.7	120.8	124.7	108.5	−13.0%
Fixed moment plane	0°	91.4	N/A	91.4	92.9	+1.6%
	15°	94.2	94.8	94.5	93.7	−0.9%
	30°	98.8	94.2	96.5	97.7	+1.2%
	45°	106.7	106.7	106.7	108.5	+1.7%

5.1. Influence of reinforcement: FEA results

In general, two modes of deformation were observed for the C-section reinforcement (Fig. 9), where the narrow reinforcement flange under compression folds outwards (mode 1), or inwards (mode 2). The change in deformation from mode 1 to mode 2 occurs when the loading angle > 45° for boundary condition 1, and 60° for boundary condition 2. For a corrugated reinforcement, only mode 2 was observed, regardless of boundary condition or loading direction.

Moment–rotation curves for both boundary conditions at 0 and 90° are presented in Fig. 10 and Fig. 11, which clearly shows the bending moments are significantly higher than the unreinforced beam throughout the whole collapse sequence. Additionally, when the beams are subjected to 0° bending load (i.e. the widest reinforcement flange is under compression), the reinforcement effectively prevents the moment from dropping in the post-buckling stage. Comparing to a C-section reinforcement, the corrugated reinforcements do not show a significant difference in terms of maximum moment (between 0.2% and 2.4% higher), but in the post-buckling stage, the corrugated beams have a noticeably higher moment, representing an increase in energy absorption between 8.5 and 21.2%.

The specific energy absorption (SEA) was used to directly compare the energy absorption performance using Eq. (2):

$$SEA = \frac{Energy\ absorption}{m_{tube} + m_{reinforcement}} \tag{2}$$

where m_i, represents the mass of the tube and reinforcement respectively.

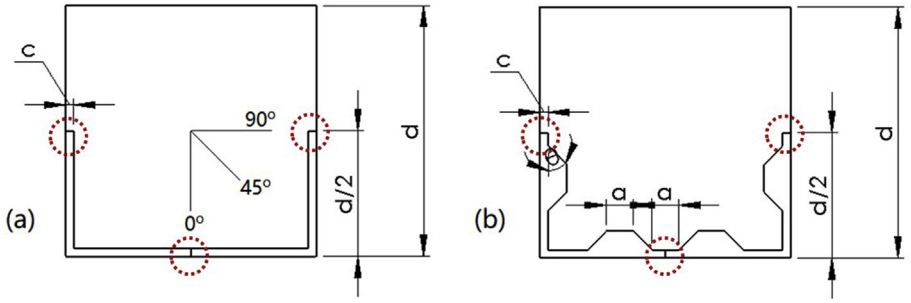

Fig. 7. Cross-sections of beams with (a) plain reinforcement and (b) corrugated reinforcement. (Circled regions denote the continuous weld lines connecting tube and reinforcement).

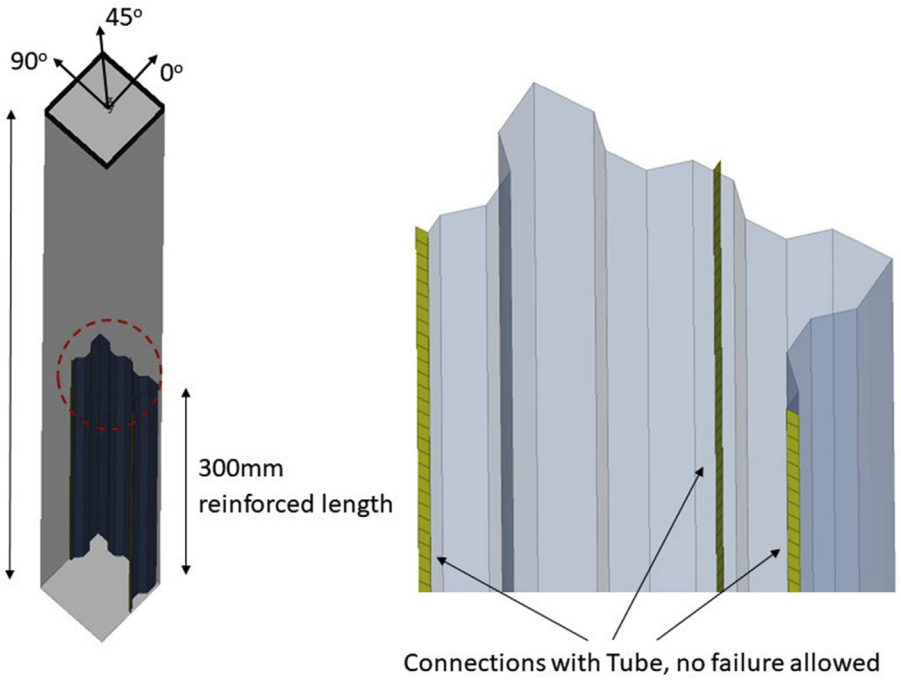

Fig. 8. Tube dimensions, detailing the connections between reinforcement insert and outer tube.

Table 3
Internal reinforcement notation and dimensions.

Dimensions	Notation	Value	Units
Width of square section beam	d	37.40	mm
Gap between the shell mid planes (outer tube and reinforcement) reinforcement – c	c	1.20	mm
Corrugation width	a	4.00	mm
Corrugation depth	b	2.83	mm
Corrugation angle	Θ	45	deg

The SEA as a function of loading direction are presented in Fig. 12, with the corrugated reinforced beams being noticeably (and consistently) higher. Additionally for the C-Section reinforcements, as the loading angle increases, the energy absorption tends to drop and to some extent, follows the trend of an unreinforced tube. However, for the corrugated reinforcement beams, the energy absorption is insensitive to load directions < 75°. These results lead to the conclusion that corrugated reinforcements offer an effective way for improving the energy absorbing performance of thin-walled beams under deep bending collapse.

6. Corrugated reinforcement: parametric study

This section presents a parametric study by varying different geometric profile parameters, in order to identify key design variables for future optimisation studies. Design variables include corrugation angle, depth and number of corrugations using the same FE model as described in Section 4.

6.1. Corrugation angle, Θ

Four corrugation angles were considered, ranging from 45 to 90° in 15° increments (Fig. 13). Corrugation angles greater than 90° were not considered as difficult to form.

Corrugation angle does not appear to noticeably influence the SEA values (Fig. 14). Considering the 45° corrugation angle as the baseline, the SEA for the other three angles varied within 1%, regardless of the boundary conditions applied to top of the beam. In terms of collapse mode, all beams behaved similarly. Despite corrugation angle not influencing the energy absorbed or failure mode, one observation is that the greater angles effectively reduces the width of corrugations, potentially allowing the reinforcement to accommodate more corrugations.

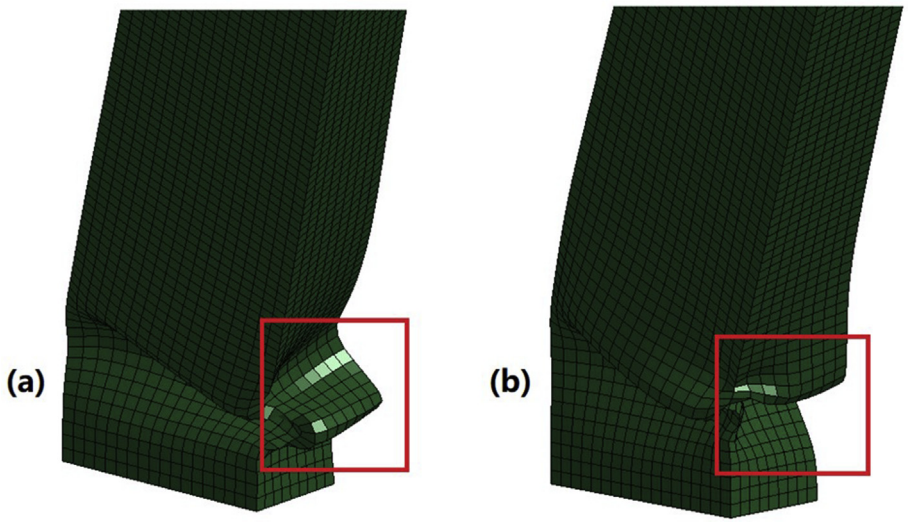

Fig. 9. (a) Deformation mode 1 and (b) deformation mode 2.

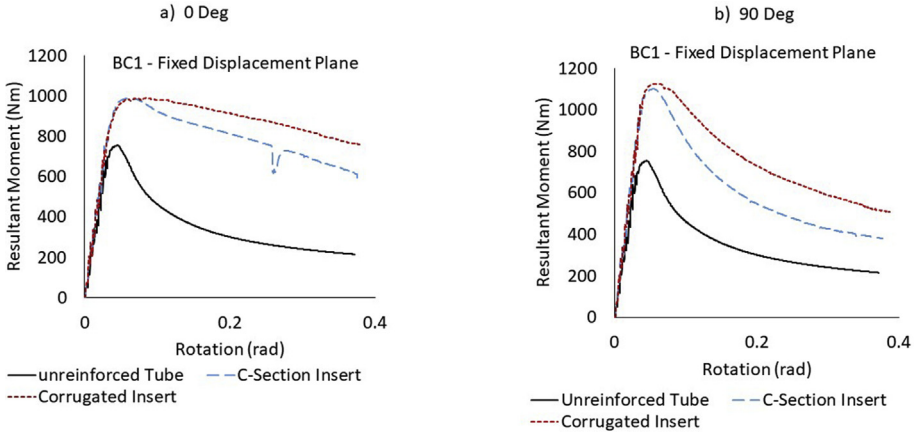

Fig. 10. Moment – rotation curves for boundary condition 1 (i.e. fixed displacement plane).

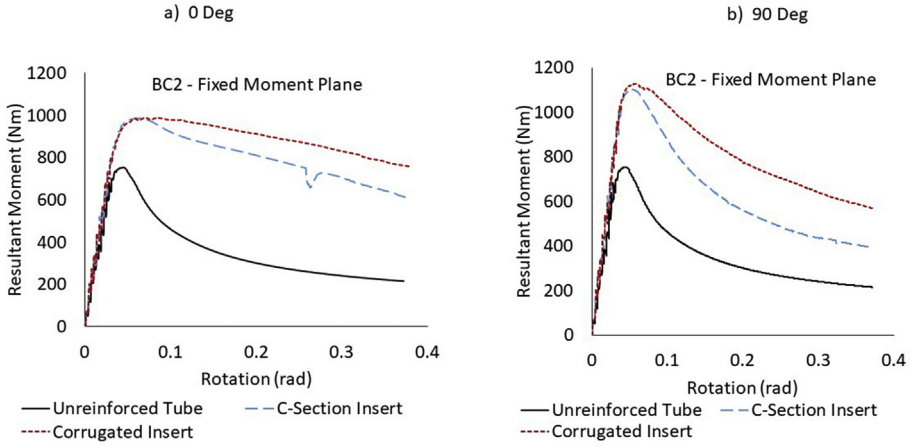

Fig. 11. Moment – rotation curves for boundary condition 2 (i.e. fixed moment plane).

6.2. Corrugation depth, b

This parameter refers to the perpendicular distance between faces of a single corrugation. Based on the dimensions in Table 3, corrugation depths of b and 1.5b were analysed for a 90° corrugation angle and compared to the C-Section (considered to be an extreme "zero" depth corrugated beam, i.e. b = 0).

The SEA as a function of corrugation depth and load angle are presented in Fig. 15. For fixed moment plane beams, increasing the corrugation depth from zero to b results in an SEA increase of +20.9%, and increasing to a depth of 1.5b, causes an additional SEA increase of +5.4%. Similarly, for fixed displacement plane beams, SEA of depths of b and 1.5b were 21.2% and 26.9% higher than the C-section respectively. Additionally, another advantage of a high corrugation depth is a

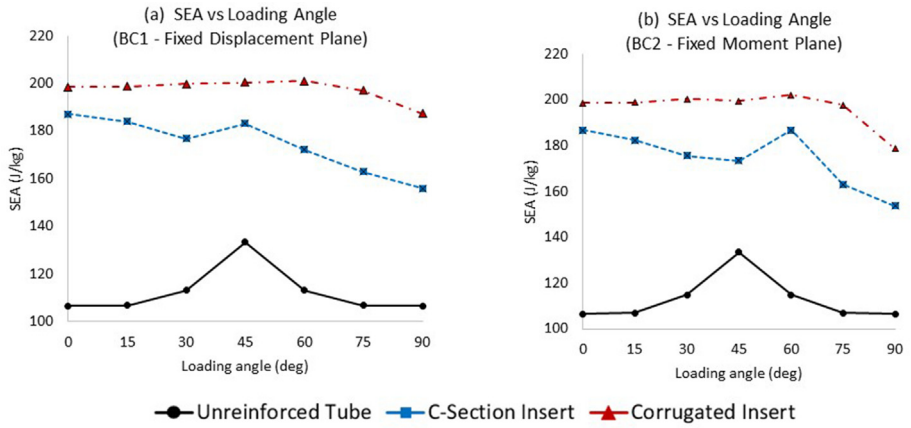

Fig. 12. SEA versus loading angle for (a) fixed displacement plane and (b) fixed moment plane boundary conditions.

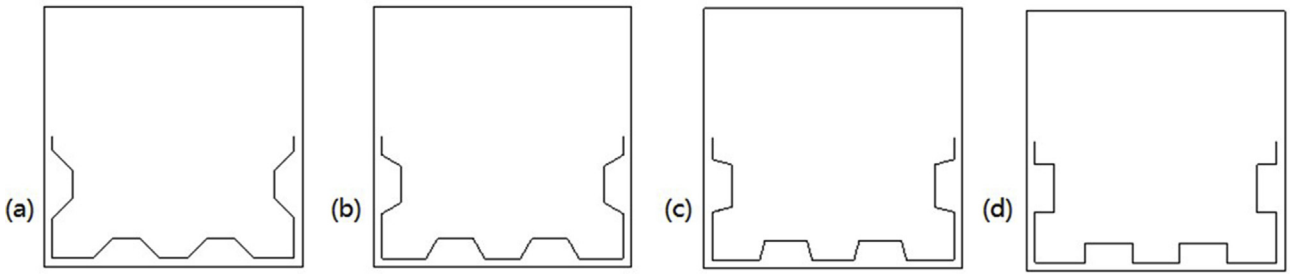

Fig. 13. Cross-sectional profiles with (a) 45° (b) 60° (c) 75° and (d) 90° corrugation angles.

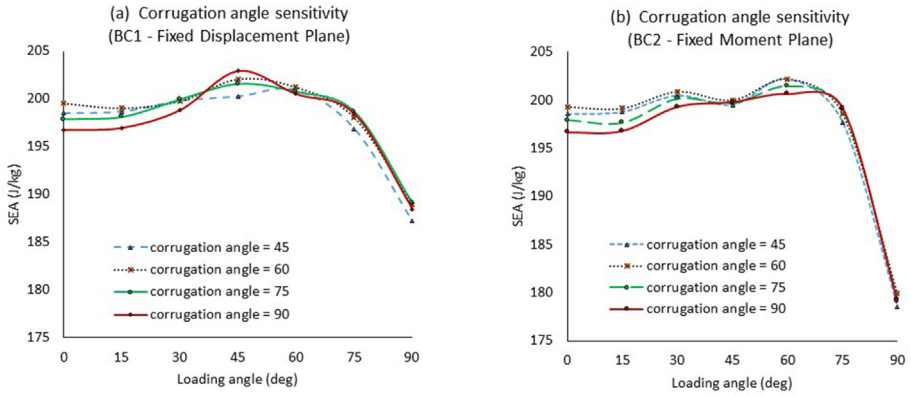

Fig. 14. Corrugation angle sensitivity: SEA vs load angle (a) fixed displacement plane and (b) fixed moment plane conditions.

higher SEA at larger loading angles.

6.3. Number of corrugations

For the baseline reinforcement, four corrugations were defined, which were doubled to investigate its influence on SEA (Fig. 16). For both boundary conditions, the SEA of an eight-corrugation insert is 6.5% higher than with four corrugations. The increase in SEA is prominent when the loading angle is at least 45°, which is consequence of having narrower corrugations (as the corrugation number increase), resulting in smaller effective buckling lengths, which subsequently strengthened the reinforcement on the compression side of the beam (see highlighted inset image in Fig. 16(a)).

7. Conclusions

In this study, a novel concept of employing corrugated features in reinforcements was proposed for the purpose of improving energy absorption of thin-walled beams under deep bending collapse. A series of finite element simulations were performed to predict the behaviour of thin-walled beams with different configurations (unreinforced, C-section and corrugated reinforcements), subjected to uniaxial and bi-axial loads.

Key findings include:

- Corrugated internal reinforcements provide an effective way of increasing the buckling strength of a cross section. This favourable response is due to an increased amount of material undergoing plastic deformation, which consequently improves performance of the beam undergoing post buckling and deep collapse.
- Comparing to a C-section reinforcement, corrugated reinforcements do not show a significant difference in terms of maximum moment (between 0.2% and 2.4% higher), but in the post-buckling stage, the corrugated beams have a noticeably higher moment, representing potential increases in energy absorption of up to 21%.
- For corrugated inserts, the energy absorption is insensitive to load

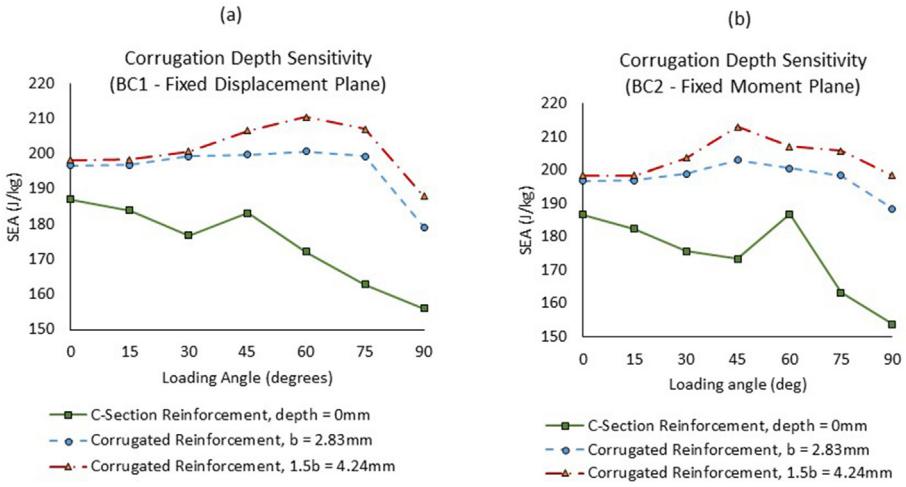

Fig. 15. Influence of corrugation depth on SEA as a function of load angle for a 90° corrugation angle, SEA vs load angle (a) fixed displacement plane and (b) fixed moment plane tubes.

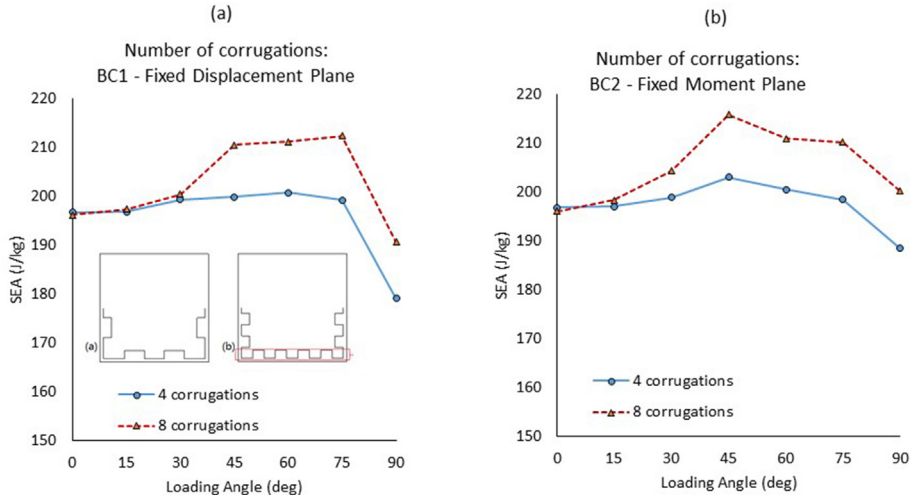

Fig. 16. Number of corrugations sensitivity: SEA vs load angle (a) fixed displacement plane and (b) fixed moment plane for a 90° corrugation angle and depth = b.

directions up to 75°. Corrugation angle also does not significantly influence the energy absorption performance of reinforced tubes.

- Increasing either corrugation depth, or the number of corrugations can increase the specific energy absorption of reinforced tubes, especially when the loading angle is large. However, greater corrugation depth and increased number of corrugations may cause manufacturing difficulties.
- This corrugated reinforcement concept is applicable to vehicle and aircraft passive safety, with the requirement that the considered geometries are manufacturable from Aluminium Alloys sheet through the HFQ process.

Acknowledgements

This research was funded by Innovate UK; Grant Number 113153 and the Advanced Propulsion Centre (APC), as part of the APC7 Rapid Aluminium Cost Effective Forming (RACEForm) project. The consortia comprised Impression Technologies Ltd, Gestamp Washington UK Limited (a wholly owned subsidiary of Gestamp Automoción), Innoval Technology Limited, Imperial College London and Brunel University London.

Appendix A. Supplementary data

Supplementary data to this article can be found online at https://doi.org/10.1016/j.tws.2019.106277.

References

[1] D. Kecman, Bending Collapse of Rectangular Section Beams in Relation to the Bus Roll over Problem, Cranfield University, 1979.
[2] S. Santosa, T. Wierzbicki, Effect of an ultrlight metal filler on the bending collapse of thin-walled prismatic columns, Int. J. Mech. Sci. 41 (8) (1999) 995–1019.
[3] H. Zarei, M. Kroger, Bending behaviour of empty and foam-filled beams: structural optimization, Int. J. Impact Eng. 35 (6) (2008) 521–529.
[4] J. Zhang, H. Zhou, L. Wu, G. Chen, Bending collapse theory of thin-walled twelve right-angle section beams filled with aluminium foam, Thin-Walled Struct. 94 (2015) 45–55.
[5] J. Xiao, J. Fang, G. Sun, Q. Li, Crashworthiness design for functionally grade foam-filled bumper beams, Adv. Eng. Software 85 (2015) 81–95.
[6] I. Duarte, L. Vesenjak, I. Krstulovic-Opara, I. Anzel, J. Ferreira, Manufacturing and bending behaviour of in situ foam-filled aluminium alloy beams, Mater. Des. 66 (2015) 532–544.
[7] X. Zhang, H. Zhang, Static and dynamic bending collapse of thin-walled square beams with beam filler, Int. J. Impact Eng. 112 (2018) 165–179.
[8] Q. Liu, X. Xu, J. Ma, J. Wang, Y. Shi, D. Hui, Lateral crushing and bending responses of CFRP square beam filled with aluminium honeycomb, Compos. B Eng. 118 (2017) 104–115.
[9] Y. Xiao, Y. Hu, J. Zhang, C. Song, Z. Liu, J. Yu, Dynamic bending responses of CFRP Thin-Walled square beams filled with aluminium honeycomb, Thin-Walled Struct. 132 (2018) 494–503.

[10] Z. Wang, Z. Li, X. Zhang, Bending resistance of thin-walled multi-cell square beams, Thin-Walled Struct. 107 (2016) 287–299.
[11] Z. Wang, X. Zhang, Z. Li, Bending collapse of mult-cell beams, Int. J. Mech. Sci. 134 (2017) 445–459.
[12] X. Zhang, H. Zhang, K. Leng, Experimental and numerical investigation on bending collapse of embedded multi-cell beams, Thin-Walled Struct. 127 (2018) 728–740.
[13] A. Teter, Z. Kolakowsi, Buckling of thin-walled composite structures with intermediate stiffeners, Compos. Struct. 69 (4) (2005) 421–428.
[14] M. Obst, D. Kurpisz, P. Paczos, The experimental and analytical investigation of torsion phenomenon of thin-walled cold formed channel beams subjected to four-point bending, Thin-Walled Struct. 106 (2016) 179–186.
[15] C. Liang, J. Wang, M. English, D. Mynors, Behaviour of cold-formed dimpled columns under lateral impact, Eng. Struct. 163 (2018) 167–176.
[16] K. Magnucki, P. Paczos, Theoretical shape optimization of cold-formed thin-walled channel beams with Drop flanges in pure bending, J. Constr. Res. 65 (8–9) (2009) 1731–1737.
[17] E. Magnucka-Blandzi, K. Magnucki, Buckling and optimal design of cold-formed thin-walled beams: review of selected problems, Thin-Walled Struct. 49 (5) (2011) 554–561.
[18] H. Yin, Y. Xiao, G. Wen, Q. Qing, Y. Deng, Multiobjective optimization for foam-filled multi-cell thin-walled structures under lateral impact, Thin-Walled Struct. 94 (2015) 1–12.
[19] J. Brown, The Collapse Fo Thin-Walled Rectangular Beams in Biaxial Bending, MSc Thesis Cranfield Institute of Technolgy, 1980.
[20] J. Brown, G. Tidbury, An investigation of the collapse of thin-walled rectangular beams in biaxial bending, Int. J. Mech. Sci. 25 (9–10) (1983) 733–746.
[21] J. Miles, The Application of Finite Element Method to Vehicle Collapse Analysis, Phd Thesis Cranfield University, 1977.
[22] Livermore Software Technology (LSTC), LS-DYNA keywords user's manual - volume 1," LSTC, California, LS-DYNA R10 vol. 0, (2017).
[23] O. Gulavani, K. Hughes, R. Vignjevic, Explicit dynamic formulation to demonstrate compliance against quasi-static aircraft seat certification loads (CD25.561) - Part 1: influence of time and mass scaling, Proc. IME G J. Aero. Eng. 228 (11) (2013) 1982–1995.
[24] A. Sadegh, W. Worek, Marks' Standard Handbook for Mechanical Engineers, twelfth ed., McGraw Hill Education, 18th November, 2017.
[25] T. Lu, Energy Absoprtion of Structures and Materials, Woodhead Press, Cambridge, England, 2003.
[26] L. Guo, J. Yu, Dynamic bending response of double cylindrical beams filled with aluminium foam, Int. J. Impact Eng. 38 (2–3) (2011) 85–94.